Communication—supercritically-dried membranes and powders of >90% porosity silicon with pore volumes exceeding 4 cm^3g^{-1}

Nekovic, Elida; Storey, Catherine J.; Kaplan, Andre; Theis, Wolfgang; Canham, Leigh T.

DOI:
10.1149/2162-8777/ab69b1

Supercritically-dried membranes and powders of >90% porosity silicon with pore volumes exceeding 4cm^3/g

Elida Nekovic [z], Catherine J. Storey, Andre Kaplan, Wolfgang Theis and Leigh T. Canham^.
[z] exn694@student.bham.ac.uk ^l.t.canham@bham.ac.uk

School of Physics & Astronomy, University of Birmingham, Edgbaston, Birmingham, B15 2TT, United Kingdom

Abstract

Porous silicon structures can display full biodegradability into orthosilicic acid and are under development for medical uses such as drug delivery. Here we demonstrate optimized electrochemical etching and drying conditions to achieve ultrahigh porosity structures ("silicon aerocrystals"), which should enable ultrahigh nanostructured drug payloads. Supercritical drying (SCD) of detached 41 to 210 micron thick films from etched p+ wafers generates structures with pore volumes 3.5 to 5.13 cm^3/g, average pore diameters of 29nm to 35nm and surface areas 425 to 549 m^2/g. For anodized p+ wafers, the benefits of SCD vs air drying (AD) are primarily elevated pore volumes.

Key words: porous silicon, electrochemical etching, mesoporous, pore volume, supercritical drying.

Introduction

Mesoporous materials are receiving increasing attention for drug delivery.[1,2]
Required properties include biocompatibility, excellent control of morphology and thereby the ability to tune the delivery of therapeutic levels of drug, either by restricted diffusion, matrix biodegradability or a combination of the two. One key parameter is the drug payload, the amount of drug that can be entrapped within the mesoporous matrix, since this determines how much material needs to be administered to achieve therapeutic drug levels. Reservoir systems for drug delivery typically achieve higher payloads than matrix systems but can suffer from concerns regarding in-vivo "dose dumping" when carrying potent actives. Matrix systems that are mesoporous and biodegradable can minimize such risks and also nanostructure drugs entrapped within.[1]
Electrochemical etching of bulk silicon can realize biodegradable mesoporous silicon with highly tunable morphology.[2,3] The physical integrity of nanostructures created by such wet processes can however be compromised by how they are dried prior to use, due to the huge capillary forces accompanying liquid evaporation from nanoscale pores.[4] It has previously been shown that very high porosity, thin layers on wafers [5], very high surface area powders [6] and luminescent structures of high quantum efficiency [7] can be realized via drying with supercritical fluids [8], a technique that avoids the capillary forces of air drying.
Here, we report typical anodization conditions and the highly beneficial effects of using supercritical drying, for creating either optical quality and thick membranes or microparticulate powders of record high pore volumes. We were particularly interested in exploring the limits of porosity (pore volume) for nanostructured mesoporous silicon and thereby the potential for very high small molecule drug payloads. Table 1 shows the conversion of gas adsorption derived pore volumes to porosity, based on the density of silicon (2.33gcm^{-3}). Typical drug payloads reported to date for porous silicon [9,10] and other mesoporous materials [11,12] lie in the range 10-50wt% corresponding to partial or near filling of pore volumes in the range

50 to 75% porosity. For all mesoporous materials, at porosities above 90% however, the pore volumes and hence potential wt% payloads of drugs rise dramatically. We illustrate this by including the potential payloads of a common model drug, ibuprofen, assuming complete pore filling and a drug density of 1.0 g cm^{-3}. Virtually complete filling of pore volume has been previously demonstrated in porous silicon for selected drugs via melt intrusion techniques.[13] Ibuprofen, a popular model drug, is also amenable to melt intrusion because of its low melting point of 78 ˚C. Drug impregnation of mesoporous materials are an attractive route to stabilizing amorphous drugs, preventing recrystallization through physical confinement.[14] However, pore volumes are normally in the range 0.7-1.5 cm^3/g and thus drug payloads are often restricted to less than 40wt%. This has negative implications on the in-vivo biomaterial doses and thereby potential toxicity of formulations required to deliver therapeutic drug doses. The record high pore volumes (4-5ml/g) reported here should enable high drug payloads and formulations of improved efficacy.

Experimental

Anodization and membrane preparation.

Heavily doped p-type 6 inch diameter wafers of 0.005 to 0.02 Ωcm resistivity were anodized in a double-tank cell in an electrolyte containing equal volumes of 40wt% HF and ethanol ("20% ethanoic HF"). Galvanostatic etching was used with current densities in the range 72 to 108 mA/cm^2. The interface uniformity of porous silicon multilayers has been improved by using "etch stops", short periods of zero bias, for electrolyte replenishment. [15] With multilayer fabrication, porosity is modulated with depth by using alternating high and low current densities in a cyclic fashion. Pulsed etching was purported to also improve the depth uniformity of thick layers made under constant current density. [16] In both cases however, total anodization times are increased significantly, increasing the overall negative porosity gradient from the top to the bottom of the layer that arises from secondary chemical etching. Etch stops during anodization were not used here. The range of anodization times was from 18.5 minutes to 74 minutes.

Membranes were "lifted off" the wafer by using elevated current pulses of 165 mA/cm^2 at the end of anodization. Membrane detachment occurs in the electrolyte rinse bath consisting of pure ethanol. Some detached high porosity membranes were subjected to secondary chemical etching in a 10% "ethanoic HF" (1 volume of 40wt%HF to 3 volumes of 100% ethanol) solution for periods ranging from 1 to 6 hours to raise their porosity further.

Storage and Drying techniques

Membrane flakes were collected and stored in ethanol: each wafer providing two batches – one for subsequent air drying at room temperature; the other for supercritical drying (SCD) process in a Quorum Technologies Limited K850 critical point drier. Storage times in ethanol prior to drying were in the range 24 to 120 hours. The standardized SCD process has been described in detail previously [6] but in summary involved flushing ethanol out with liquid CO_2, converting the liquid CO_2 to supercritical CO_2, further flushing with supercritical CO_2, and then venting the supercritical fluid. The process took 65 to 85 minutes.

Gas adsorption/desorption analysis

Nitrogen gas adsorption/desorption was used to determine pore volume, surface area and average pore diameter for each powder, using a Micromeritics Tristar 3020. Computational analysis of the isotherms yielded pore volume based on the Barrett-Joyner-Halenda adsorption method; surface area via the Brunauer-Emmett-Teller method; and average pore diameter was estimated from the adsorption branch (4V/A) method by BET. Pore size distributions were from computational analysis of the adsorption branch using the BJH

method. Pore volume values obtained from gas adsorption were converted to porosities and compared to those obtained from gravimetric data. Gravimetric porosity and thickness were determined from calculations using the wafer diameter and density of silicon with 3 weights w_i=initial weight of the Si wafer before anodization; w_f=final weight of the Si wafer (after pSi has been detached); w_{psi}=weight of porous silicon membrane.

Electron microscopy

High Resolution Scanning Electron Microscopy (HRSEM) was used to study morphology using a Philips XL30 ESEM-FEG microscope and 20keV electron beam with prior nm-scale Au coating of membrane surfaces to minimize beam charging.

Results and Discussion

The colours of the detached porous silicon membranes are a function of their porosity and thickness. Figure 1 shows how the colour evolves with increasing porosity at a given thickness from (a) the grey of bulk silicon to dark brown to orange-brown to a light tan colour, even for high thicknesses of tens of microns. The membranes with porosities greater than 90% were mechanically very fragile but had good optical transparency, and low enough light scattering to read text through them as shown in figure 2. The mode of drying was found to have a pronounced effect on membrane structure. The air-dried structures suffered from skeleton shrinkage and cracking at various length scales, as shown in figure 3. This resulted in air-dried structures having consistently lower pore volumes, as quantified by gas adsorption data. Table 2 summarizes porosity and thickness values from gravimetric data, with surface area and mean pore sizes from gas adsorption data analysis.

General trends apparent are that the SCD membranes have substantially higher pore volumes and mean pore sizes but only slightly higher surface areas than the AD equivalents. This is in contrast to anodized p- wafers where the primary benefit has been shown to be greatly enhanced surface areas. [6]

All 5 SCD membranes had porosities of 89% or higher, as measured by gas adsorption with pore volumes in the range 3.5 - 5.1ml/g. Figures 4a contrasts the isotherms of AD and SCD UoB 20, the structure with a record high pore volume greater than 5ml/g. The corresponding extracted pore size distributions are shown in figure 4b. In the SCD structure pores up to 100nm in diameter make a significant contribution whilst in the AD structure the majority of pores are under 50nm wide. This 92.3% porosity structure was examined by HRSEM and example plan view and cross-sectional images are shown in figure 5a and 6a. Gravimetric data on thickness was found to consistently yield slightly higher values than SEM values, as expected due to some membrane thinning during anodization and chemical etching which becomes more and more significant, the higher the porosity and thickness (etch duration) of the membranes.

The plan view HRSEM image (figure 5a and b) of the bottom faces of the membranes reveal a honeycomb network of interconnected silicon nanowire of strongly fluctuating width with mean diameters 51 +/- 10nm. Their morphology appears similar to that of the much smaller “quantum wires” of width <3nm observed by HRTEM in high porosity luminescent porous silicon.[15] However the fluctuating nanowire widths evident in figure 5 may be a consequence of the Au coating used here, and this needs further investigation. Such

Au coatings will also lead to an underestimate of porosity and pore sizes and an overestimate of mean silicon nanowire width generated under these etching conditions.

For ultrahigh porosity structures created by adjacent cylindrical pores merging into 3D voids, the definition of a ”pore” becomes ambiguous. The voids between nanowires on the very outer gold-coated surface of the UoB20 membrane have a wide size distribution in the diameter range 30-130nm with a mean value of 72nm. Cross-sectional HRSEM images of gold-coated fracture surfaces (figure 6) gave a lower mean nanowire to nanowire separation of 56 +/- 20nm. Gas adsorption data, reflecting the entire volume of the same membrane and on as-etched structures gave a mean “pore” size of 31nm (table 2). We expect both membrane faces to have significantly larger void dimensions than the membrane bulk because the top face has received the longest chemical etch during anodization and the bottom face received the higher current pulse to achieve “lift off”. Future studies plan to utilize image processing techniques [18] to better compare estimates of overall porosity, pore/void size and skeleton size distributions from both HRTEM and HRSEM with that of gas adsorption analysis. This will necessitate the avoidance of even ultrathin (<4nm) Au coatings.

Cross-sectional HRSEM was also used to check for micro-cracking within the membranes, qualitatively assess surface roughness and check the accuracy of gravimetric techniques [19] in measuring overall porosity and thickness of these aerocrystal structures. Figure 6 shows images for the highest porosity (UoB20) structure. All SCD membranes had far better structural integrity throughout their thicknesses, although they are mechanically fragile (cf. macro-crack in figure 2).

Multiple measurements yielded mean thicknesses of 189 microns (UoB20) and 39.6 microns (UoB60/61), in comparison with the gravimetric values of 195 microns and 41.5 microns respectively. The gravimetric method assumes no layer thinning during etching and thus overestimates thickness by 3 % (UoB20) and 5% (UoB60/61).

This study has also shown a general trend with anodized p+ wafers in substantially higher pore volumes of SCD membranes and mean pore sizes but only slightly higher surface areas than the AD equivalents. This is in contrast to anodized p- wafers where the primary benefit has been shown to be greatly enhanced surface areas.[6]

Summary

We have identified the electrochemical etching and drying conditions that achieve both ultrahigh porosity and thick membrane structures suitable for silicon aerocrystal particle generation. Mesoporous membranes with porosities exceeding 90% and surfaces areas in the range 425-549m^2/g can be achieved directly under specific anodization conditions, or via a two-step process of anodization plus subsequent chemical etching.

We have reported the highest pore volumes (4-5ml/g) achieved to date in mesoporous silicon membranes. Supercritical drying with carbon dioxide has shown to be beneficial over drying from ethanol in preserving the highest pore volumes and surface areas generated by particular etching conditions.

We predict that such silicon aerocrystals will support very high drug payloads in future microparticle and nanoparticle-based drug delivery formulations. Such drug loading studies are currently in progress.

Acknowledgments

EN would like to thank the School of Physics & Astronomy at the University of Birmingham for financial assistance during her studies.

References

1. P. Yang, S. Gai and J. Lin, Chem. Soc. Rev. 41, 3679-3698 (2012).
2. R .J. Martin-Palma, J. Hernández-Montelongo, V. Torres-Costa, M. Manso-Silván and A. Muñoz-Noval Á, Expert Opinion Drug Delivery 11(8) 1273-1283 (2014).
3. M. J. Sailor, Porous Silicon In Practice: preparation, characterisation and applications. Wiley VCH (2012).
4. D. Bellet and L. T. Canham., Adv.Mater. 10(6) 487-490 (1998).
5. L. T. Canham, A. G. Cullis, C. Pickering, O. D. Dosser, T. I. Cox and T. P. Lynch, Nature 368,133 (1994).
6. A. Loni, L. T. Canham, T. Defforge and G. Gautier, ECS J.Solid State Sci.Technol. 4(8)289-292 (2015).
7. J. Joo, T. Defforge, A. Loni, D. Kim, Z. Y. Li, M. J. Sailor, G. Gautier and L. T. Canham, Appl. Phys. Lett. 108, 153111 (2016).
8. A. I. Cooper, Adv. Mater. 15(13) 1049-1059 (2003).
9. J. Salonen, L. Laitinen, A. M. Kaukonen, J. Tuura, M. Björkqvist, T. Heikkilä, K. Vähä-Heikkilä, J. Hirvonen and V. P. Lehto, J.Controlled Release. 108, 362-374 (2005).
10. J. Riikonen, E. Mäkilä, J. Salonen and V. P. Lehto, Langmuir 25(11) 6137-6142 (2009).
11. C. Charnay, S. Bégu, C. Tourné-Péteilh, L. Nicole, D. A. Lerner and J. M. Devoisselle, Eur.J.Pharma.Biopharma. 57, 533-540 (2004).
12. J. Anderson, J. Rosenholm, S. Areva and M. Lindén, Chem.Mater. 16, 4160-4167 (2004).
13. A. Loni in Handbook of Porous Silicon. 2nd Ed., L.Canham, Editor p945-950 Springer Reference, Switzerland (2018).
14. E. Makila, M. P. Ferreira, H. Kivelä, S. M. Niemi, A. Correia, M. A. Shahbazi, J. Kauppila, J. Hirvonen, H. A. Santos and J. Salonen, Langmuir, 30, 2196-2205 (2014).
15. S. Billat, M. Thonissen , R. Arens Fischer, M. G. Berger, M. Kruger, H. Luth, Thin Solid Films 297(1–2):22–25 (1997).
16. X. Y. Hou, H. L. Fan, F. L. Zhang, M. Q. MQ, M. R. Yu, X. Wang, Appl Phys Lett 68(17):323–2325 (1996).
17. A.G.Cullis and L. T. Canham, Nature 353 , 335 (1991).
18. P.Elia, E. Nativ-Roth, Y. Zeiri, Z. Porat, Microporous and Mesoporous Materials 225 465 (2016).
19. D. Brumhead, L. T. Canham, D. M. Seeking and P. J. Tufton, Electrochemica Acta 38, 191-197 (1993).

Tables

Porosity (void fraction)	Pore Volume (ml/g)	Maximum drug (Ibuprofen) payload achievable (wt%)
50%	0.43	30
60%	0.65	39
70%	1.0	50
80%	1.7	63
90%	3.8	79
95%	8.1	89

Table 1. Pore volumes, porosities and potential drug payloads in porous silicon.

Sample Code	*Thickness (μm) (gravimetric)*	*Porosity (%) (gravimetric)*	*Pore volume (ml/g) : AD/SCD*	*Porosity from pore volume (%) AD/SCD*	*Surface area(m^2/g): AD/SCD*	*Mean Pore size (nm): AD/SCD*
UoB 60/61	*41.0*	*86.7*	*3.05/4.55*	*87.6/91.4*	*517/520*	*19.6/35.0*
** UoB 30*	*145*	*NM*	*1.34/4.22*	*75.7/90.8*	*322/425*	*16.7/33.9*
UoB 49	*174*	*89.8*	*2.83/3.52*	*86.8/89.1*	*459/462*	*24.7/30.5*
UoB 20	*195*	*NM*	*2.65/5.13*	*86.0/92.3*	*520/549*	*16.3/31.3*
UoB 40	*210*	*92.8*	*1.88/4.24*	*81.4/90.8*	*478/497*	*12.3/28.8*

Table 2. Gas adsorption and gravimetric data of five supercritically dried membranes and their air-dried equivalents. UoBXX" values are wafer batch codes representing distinct anodization runs at the University of Birmingham (UoB). *"NM": not measured. *UoB 30 is fabricated via anodization and further chemical etching for 5.5 hours and the rest of the membranes are via anodization only.*

Figures

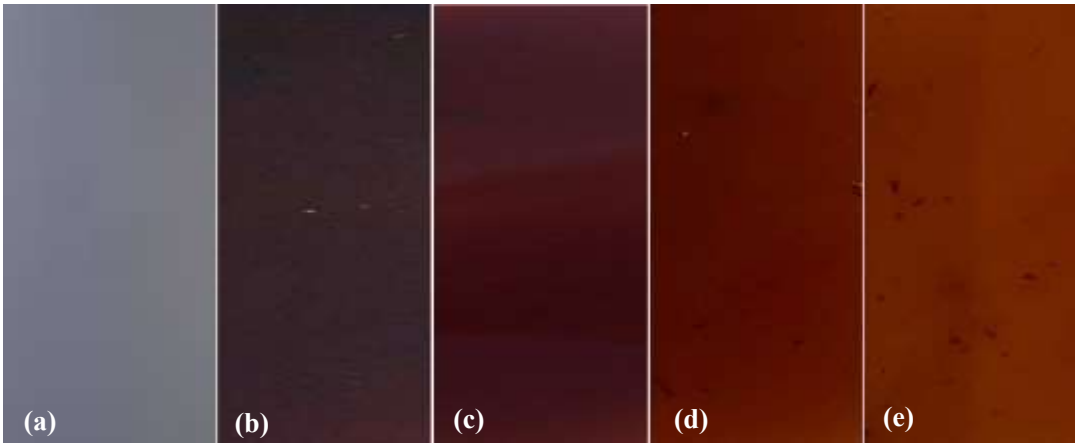

Figure 1. Optical images of Si wafer (thickness of 650 microns) and membranes of varying porosity but constant thickness of 55 microns. (a) 0% (bulk Si) (b) 84% (c) 87% (d) 90% (e) 93%. The images (b-e) are from an anodized membrane of 81% porosity that was etched in 10% ethanoic HF for increasing periods of 1,2,3 and 5 hours, respectively.

Figure 2. Optical image of an ultrahigh porosity membrane (porosity 93%, thickness 55 micron) during in-situ etching in 10% ethanoic HF.

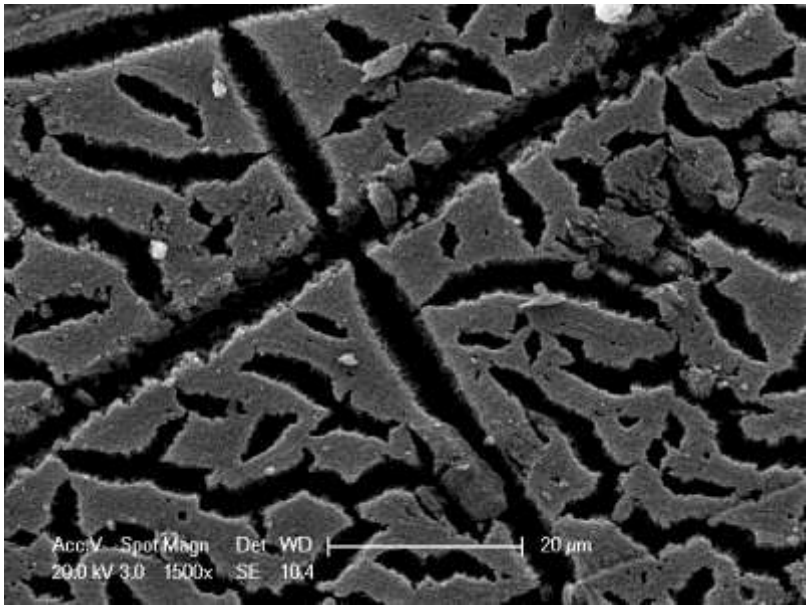

Figure 3. HRSEM plan view image of the upper face of a 91% porosity membrane (UOB30) subjected to air drying via ethanol evaporation. Such severe shrinkage and cracking was not observed in either plan view or cross-sectional SEM images of SCD membranes.

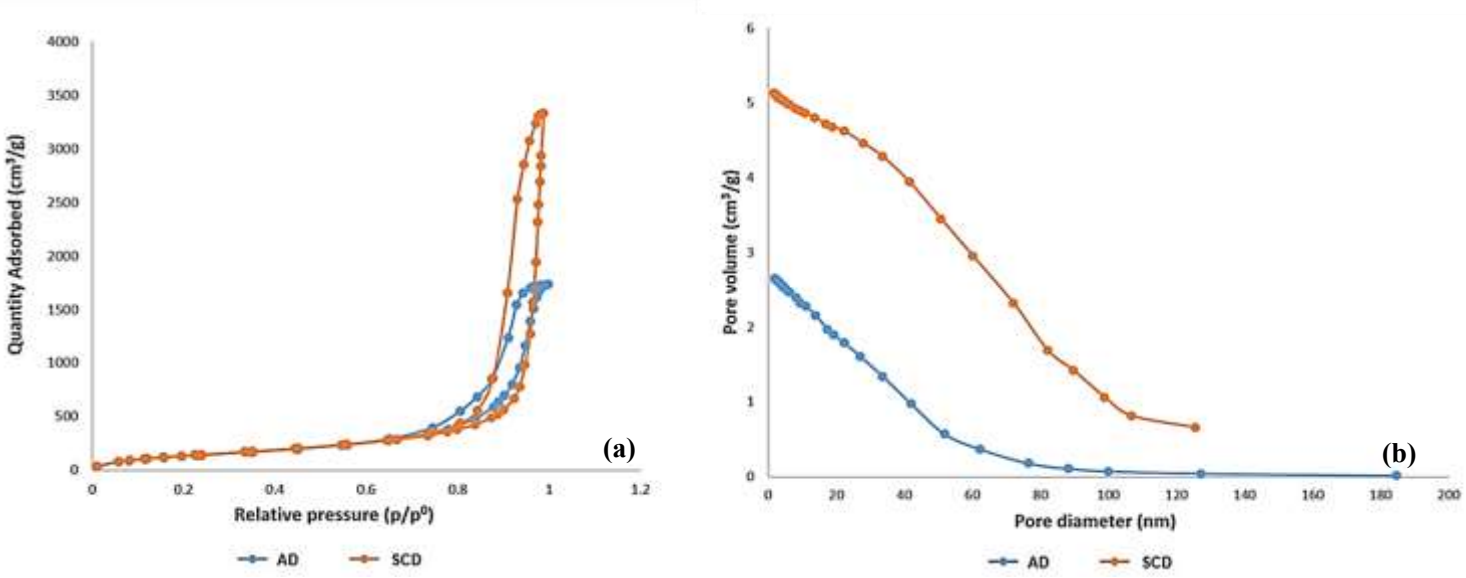

Figure 4. (a) Isotherms for air dried structure (AD) and its supercritically dried (SCD) equivalent of UoB 20. (b) *Pore size distributions (incremental pore volume) for air dried structure (AD) and its supercritically dried (SCD) equivalent of UoB 20.*

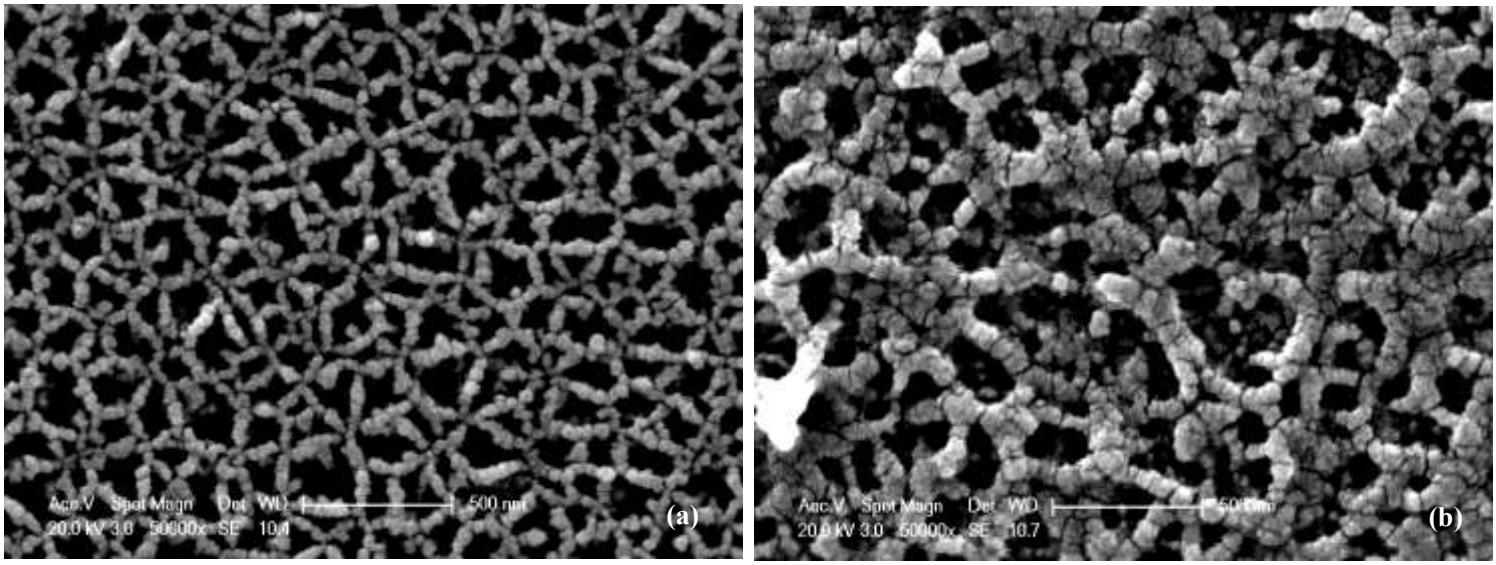

Figure 5. HRSEM plan view images of (a) SCD UoB 20 and (b) SCD UoB 30 membranes. The membrane faces were coated with nm thick gold layers to minimize beam charging, so the apparent void dimensions and porosity are lower than those produced by etching.

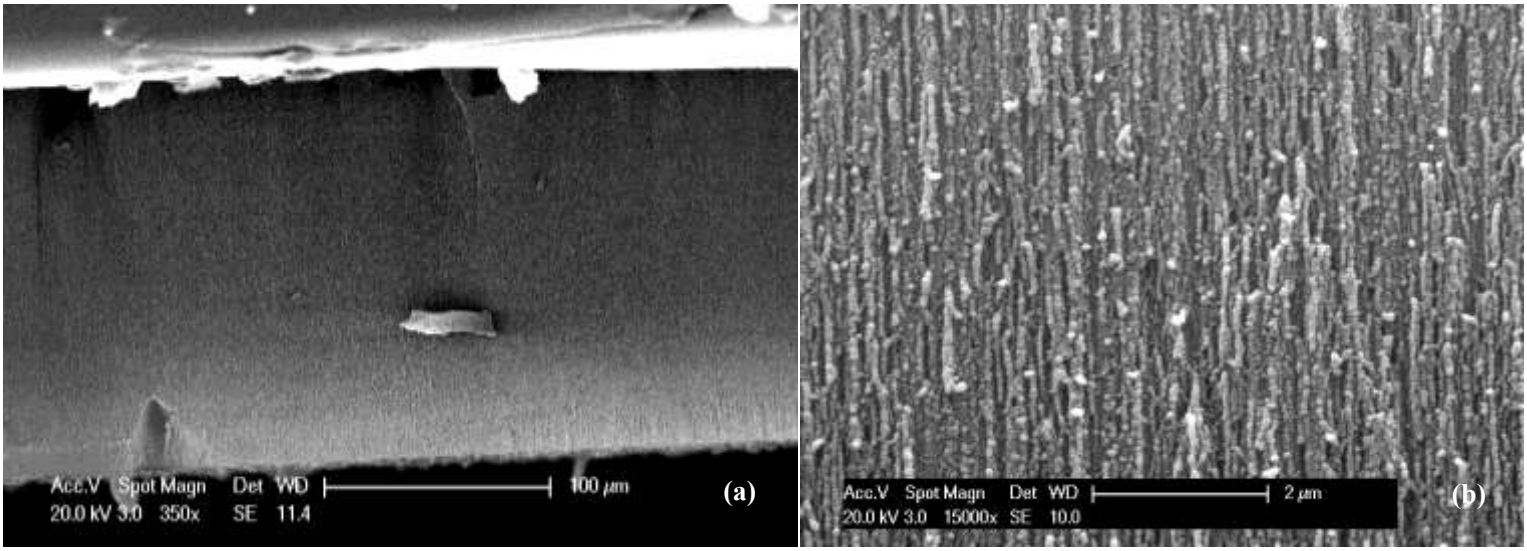

Figure 6. HRSEM cross-sectional images of SCD UoB 20 membrane at (a) low magnification showing entire thickness and (b) higher magnification showing pore directionality. The freshly cleaved surface received a nm thick Au coating which lowers the apparent porosity in (b).